

Dear Dr. Hrachowitz,

Thank you for the prompt evaluation of our revised manuscript and the positive assessment. In regards to your response regarding the benchmark: yes, we do indeed briefly compare to the time invariant parameter case and this can be considered a benchmark. We apologise for the confusion here; our intent was that no benchmark was used in investigating the impact of the model structure on the performance of the time varying parameter model, which is the main focus of the paper. The majority of the discussion is devoted to comparing the output from state and parameter updating (so called LL Dual EnKF with HBV or HyMOD) and time varying parameter model with no state updating (TVP-HBV and TVP-HyMOD).

We have added in the following statements as per your requests. Specifically, additional discussion has been provided to make clear that the time invariant parameter models were calibrated on pre-1979, and that the comparisons have been made for the time invariant parameter model evaluated over the post 1979 period. Additionally, the improvement has been quantified using the NSE.

In the methods section (Section 3.2.2, lines 348-351 of manuscript with tracked changes):

*“Joint state and parameter estimation was undertaken for the Nammuc Catchment over the period 1980 to 2004 by assimilating streamflow observations into the HyMOD and HBV models at a daily time step. Additionally, simulations using the time invariant parameters obtained from calibration over the period 1973-1979 were generated for 1980 to 2004, for comparison.”*

In the results section (Section 4, lines 463-470 of manuscript with tracked changes):

*“Streamflow predictions from the LL Dual EnKF (i.e. with state and parameter updating) for both the HyMOD and HBV are generally of similar quality and superior to those from the respective time invariant parameter models that have been calibrated on pre-change data (1975-1979), although a slight bias in baseflow predictions from HyMOD is evident (see for example Figure 6). The Nash Sutcliffe Efficiency of one step ahead streamflow predictions over the period 1980 – 2004 from the LL Dual EnKF is 0.87 when using HyMOD or HBV, compared to 0.76 and 0.72 for the respective time invariant parameter models evaluated over the same period. However, differences in predictions from TVP-HBV and TVP-HyMOD are more striking due to the lack of state updating.”*

We hope this clarifies any ambiguities, and we look forward to your response. Thank you for your time and consideration.

Best Regards,

Sahani Pathiraja  
Daniela Anghileri  
Paolo Burlando  
Ashish Sharma  
Lucy Marshall  
Hamid Moradkhani

# Time varying parameter models for catchments with land use

## change: the importance of model structure

Sahan Pathiraja<sup>1,2</sup>, Daniela Anghileri<sup>3</sup>, Paolo Burlando<sup>3</sup>,

Ashish Sharma<sup>2</sup>, Lucy Marshall<sup>2</sup>, Hamid Moradkhani<sup>4</sup>

<sup>1</sup>Institut für Mathematik  
Universität Potsdam  
Potsdam  
GERMANY

Email: [pathiraja@uni-potsdam.de](mailto:pathiraja@uni-potsdam.de)

<sup>2</sup>Water Research Centre  
School of Civil and Environmental Engineering  
University of New South Wales  
Sydney, NSW  
AUSTRALIA

<sup>3</sup>Institute of Environmental Engineering  
ETH Zurich  
Zurich  
SWITZERLAND

<sup>4</sup>Department of Civil, Construction and Environmental Engineering  
University of Alabama  
Tuscaloosa, Alabama  
USA

- Deleted: .

Deleted: ¶

## 1   **Abstract**

2   Rapid population and economic growth in South-East-Asia has been accompanied by extensive land  
3   use change with consequent impacts on catchment hydrology. Modelling methodologies capable of  
4   handling changing land use conditions are therefore becoming ever more important, and are  
5   receiving increasing attention from hydrologists. A recently developed Data Assimilation based  
6   framework that allows model parameters to vary through time in response to signals of change in  
7   observations is considered for a medium sized catchment (2880 km<sup>2</sup>) in Northern Vietnam  
8   experiencing substantial but gradual land cover change. We investigate the efficacy of the method  
9   as well as the importance of the chosen model structure in ensuring the success of a time varying  
10   parameter method. The method was used with two lumped daily conceptual models (HBV and  
11   HyMOD) that gave good quality streamflow predictions during pre-change conditions. Although both  
12   time varying parameter models gave improved streamflow predictions under changed conditions  
13   compared to the time invariant parameter model, persistent biases for low flows were apparent in  
14   the HyMOD case. It was found that HyMOD was not suited to representing the modified baseflow  
15   conditions, resulting in extreme and unrealistic time varying parameter estimates. This work shows  
16   that the chosen model can be critical for ensuring the time varying parameter framework  
17   successfully models streamflow under changing land cover conditions. It can also be used to  
18   determine whether land cover changes (and not just meteorological factors) contribute to the  
19   observed hydrologic changes in retrospective studies where the lack of a paired control catchment  
20   precludes such an assessment.

## 21 **1. Introduction**

22 Population and economic growth in South-East Asia has led to significant land use change, with rapid  
23 deforestation occurring largely for agricultural purposes [Kummer and Turner, 1994]. Forest cover in  
24 the Greater Mekong Sub-region (comprising Myanmar, Thailand, Cambodia, Laos, Vietnam, and  
25 South China) has decreased from about 73% in 1973 to about 51% in 2009 [WWF, 2013]. Vietnam in  
26 particular has had the second highest rate of deforestation of primary forest in the world, based on  
27 estimates from the Forest Resource Assessment by the United Nations Food and Agriculture  
28 Organization [FAO, 2005]. Such extensive land use change has the potential to significantly alter  
29 catchment hydrology (in terms of both quantity and quality), with its effects sometimes not  
30 immediate but occurring gradually over a lengthy period of time. Recent estimates from satellite  
31 measurements indicate that rapid deforestation continues in the region, although at lower rates [e.g.  
32 Kim et al., 2015]. Persistent land use change necessitates modelling methodologies that are capable  
33 of providing accurate hydrologic forecasts and predictions, despite non-stationarity in catchment  
34 processes. This is also particularly relevant for water resource management which requires reliable  
35 estimates of water availability, both in terms of volume and timing, to properly allocate the resource  
36 between different water uses and to prevent flood damages. Vietnam has built many reservoirs in  
37 the last decades and more are planned because they are considered to be fundamentally important  
38 for electricity production, flood control, water supply and irrigation, ultimately contributing to the  
39 development of the country [Giuliani et al., 2016].

40

41 The literature on land-use change and its impacts on catchment hydrology is extensive, with studies  
42 examining the effects of 1) conversion to agricultural land-use [Thanapakpawin et al, 2007;  
43 Warburton et al., 2012]; 2) deforestation [Costa et al., 2003; Coe et al, 2011]; 3) afforestation [e.g.  
44 Yang et al., 2012; Brown et al, 2013] and 4) urbanization [Bhaduri et al., 2001; Rose & Peters, 2001].  
45 Fewer studies have examined how traditional modelling approaches must be modified to handle

46 non-stationary conditions, or how modelling methods can be used to assess impacts of land use  
47 change. Split sample calibration has been used frequently to retrospectively examine changes to  
48 model parameters due to land use or climatic change [Seibert & McDonnell, 2010; Coron et al., 2012;  
49 McIntyre & Marshall, 2010; Legesse et al, 2003]. Several other studies have employed scenario  
50 modelling, whereby hydrologic models are parameterized to represent different possible future land  
51 use conditions [e.g. Niu & Sivakumar, 2013; Elfert & Borman, 2010]. A related approach involves  
52 combining land use change forecast models with hydrologic models [e.g. Wijesekara et al., 2012].  
53 However, the aforementioned approaches are unsuited to hydrologic forecasting in changing  
54 catchments, as the predicted land use change may not reflect actual changes. A potentially more  
55 suitable approach in such a setting is to allow model parameters to vary in time, rather than  
56 assuming a constant optimal value or stationary probability distribution. Many existing methods  
57 utilising such a framework require some *a priori* knowledge of the land use change in order to inform  
58 variations in model parameters (see for instance Efstratiadis, 2015; Brown et al., 2006; and Westra et  
59 al., 2014). Recent efforts have examined the potential for time varying parameter models to  
60 automatically adapt to changing conditions using information contained in hydrologic observations  
61 and sequential Data Assimilation, without requiring explicit knowledge of the changes [see for  
62 example Taver et al., 2015, Pathiraja et al., 2016a&b]. Such approaches can objectively modify  
63 model parameters in response to signals of change in observations in real time, whilst simultaneously  
64 providing uncertainty estimates of parameters and streamflow predictions. They can also be used to  
65 determine whether land cover changes (and not solely meteorological factors) contribute to  
66 observed changes in streamflow dynamics in retrospective studies where the lack of a paired control  
67 catchment precludes such an assessment.

68

69 Pathiraja et al. [2016a] presented an Ensemble Kalman Filter based algorithm (the so-called Locally  
70 Linear Dual EnKF) to estimate time variations in model parameters. The method sequentially  
71 assimilates observations into a numerical model in real time to generate improved estimates of

72 model states, fluxes and parameters based on their respective uncertainties. Its purpose is to infer  
73 changes to catchment properties (e.g. land cover change) from hydrologic observations, without  
74 prior knowledge of such changes, at the time scale of the available observations. It can therefore be  
75 used for various applications: 1) to retrospectively estimate time variations in model parameters; 2)  
76 for short-term predictive modelling (days to weeks), e.g. flood forecasting; and 3) for on-line/real  
77 time water resource management, e.g. determining releases from reservoirs in catchments with  
78 changing land cover conditions. In retrospective mode, the method is advantageous compared to  
79 split-sample calibration type approaches since no *a priori* knowledge of land use change is needed,  
80 and the modeller does not have to make somewhat arbitrary decisions about how to segregate the  
81 data. When used for prediction or forecasting, states and parameters are updated sequentially using  
82 all available observations up until the current time. These updated states and parameters are then  
83 used along with the prior parameter generating model to produce hydrologic predictions over a short  
84 time horizon. This allows one to seamlessly obtain predictions without the modeller needing to  
85 explicitly modify the model to account for any catchment changes. The efficacy of the method was  
86 demonstrated in *Pathiraja et al.* [2016b] through an application to small experimental catchments (<  
87 350 ha) with drastic land cover changes and strong signals of change in streamflow observations.

88

89 Here we investigate two issues related to the use of time varying parameter models for prediction in  
90 realistic catchments with changing land cover conditions. Firstly, we investigate the efficacy of the  
91 time varying parameter method for sparsely observed, medium-sized catchments with spatially  
92 complex and gradual land use change (occurring over months/years). Several authors have  
93 demonstrated that impacts of land use change on the hydrologic response are dependent on many  
94 factors including the type and rate of land cover conversion as well the spatial pattern of different  
95 land uses within the catchment [*Dwarakish & Ganasri, 2015; Warburton et al., 2012*]. In such  
96 situations, the effects of unresolved spatial heterogeneities in model inputs (e.g. rainfall) and the  
97 relatively less pronounced changes in land surface conditions make time varying parameter detection

98 and accurate hydrologic prediction more difficult. The second objective is to examine the role of  
99 the hydrologic model in determining the ability of the time varying parameter framework to provide  
100 high quality predictions in changing conditions. Often there may be several candidate hydrologic  
101 models (with time invariant parameters) that have similar predictive performance for a catchment  
102 when calibrated and validated over a time series of static land cover conditions [Marshall *et al.*,  
103 2006]. This work examines whether all such candidate models in time varying parameter mode are  
104 also capable of providing accurate predictions under changing conditions.

105

106 These issues are investigated for the Nammuc catchment (2880 km<sup>2</sup>) in Northern Vietnam which has  
107 experienced deforestation largely due to increasing agricultural development. It serves as an ideal  
108 test catchment to study the efficacy of the time varying parameter algorithm due to its size, spatially  
109 complex pattern of land use changes, and lack of information on the precise timing of such changes.  
110 Land cover change is estimated to have occurred at varying rates, with cropland accounting for  
111 roughly 23% between 1981 and 1994, and 52% by 2000. We also consider two lumped conceptual  
112 hydrologic models (given the availability of point rainfall, temperature, and streamflow data)  
113 operating at daily time step to address the second objective. Both models demonstrate similar  
114 performance in representing streamflow at the outlet during the pre-change calibration period  
115 (1975-1979), although their performance during/after land use change is unknown. Therefore, the  
116 effect of the model structure (i.e. model equations) on hydrologic predictions from the time varying  
117 parameter models is studied. This work represents the first application of a continuously time  
118 varying parameter approach for modelling a real medium sized catchment with no *a priori* (or partial)  
119 knowledge of the type and timing of land use change.

120

121 The remainder of this paper is structured as follows. Details of the study catchment and the impact  
122 of land cover change are analysed in Section 2. Section 3 summarizes the experimental setup  
123 including the hydrological models and the time varying parameter estimation method used. Results

124 are provided in Section 4, along with an analysis of whether the time varying model structures reflect  
125 the observed catchment dynamics. Finally, we conclude with a summary of the main outcomes of  
126 the study as well as proposed future work.

## 127 **2. The Nammuc Catchment**

128 The Nammuc catchment (2880 km<sup>2</sup>) is located in the Red River Basin, the second largest drainage  
129 basin in Vietnam which also drains parts of China and Laos. The local climate is tropical monsoon  
130 dominated with distinct wet (May to October) and dry (November to April) seasons. The wet season  
131 tends to have high temperatures (on average 27 to 29 °C) due to south-south easterly winds that  
132 bring humid air masses. Conversely, during the dry season, circulation patterns reverse carrying  
133 cooler dry air masses to the basin (leading to average temperatures of 16 to 21°C). Streamflow  
134 response is consequently monsoon driven, with high flows occurring between June and October  
135 (generally peaking in July/August) and low flows in the December to May period (Vu, 1993). Average  
136 annual rainfall at Nammuc varies between 1300 and 2000 mm (on average 1600 mm) and catchment  
137 elevation ranges between 350 and 1500 m asl. A summary of catchment properties is provided in  
138 [Table 1](#) for pre-change (prior to 1994) and post-change (after 1994) conditions. This separation was  
139 based on available land cover information as described below.

Deleted: Table 1

### 140 **2.1.Data & Land Cover Change**

141 [Figure 1](#) shows the available land cover information for the Nammuc catchment. Land cover  
142 information for the catchment is scant, we were able to locate only two sources which unfortunately  
143 do not give a complete picture over the entire time period of interest (1970 to 2004). The first land  
144 cover map refers to the period 1981-1994 and was obtained by the Vietnamese Forest Inventory and  
145 Planning Institute (<http://fipi.vn/Home-en.htm>). The second land cover map refers to year 2000 and  
146 was obtained from the FAO Global Land Cover database  
147 (<http://www.fao.org/geonetwork/srv/en/metadata.show?id=12749&currTab=simple>). A comparison

Deleted: Figure 1

150 of the two maps shows a reduction in forest cover in favor of cropland; Evergreen Leaf decreases  
151 from about 60% to 30% whilst cropland increases from about 23% to 52%. The change in land cover  
152 is patchy, although mostly concentrated in the northern part of the catchment. Because of the scant  
153 information available, it is not easy to identify the precise time period of these changes. Based on the  
154 available land cover map information and the changes to observed runoff (see Section 2.2), we posit  
155 that a period of rapid extensive deforestation occurred in early to mid-1990s.

156

157 Daily point rainfall data is available at four precipitation stations surrounding the catchment (Dien

158 Bien, Tuan Giao, Quynh Nhai and Nammuc, see [Figure 1](#)). Catchment averaged rainfall was

159 developed as a weighted sum of the four stations with weights determined by Thiessen Polygons.

160 Daily mean temperature was calculated in a similar fashion using temperature records from the 2

161 closest gauges (Lai Chau and Quynh Nhai, see [Figure 1](#)). This was used to estimate Potential

162 Evapotranspiration through the empirical temperature-latitude based Hamon PET method [*Hamon*,

163 1961]. Daily rainfall, temperature and streamflow data was provided by the Vietnamese Institute of

164 Water Resources Planning.

## 165 2.2. Impact of Land Cover Change on Streamflow

166 The annual runoff/direct runoff coefficient and Baseflow Index were used to assess the impact of

167 land cover change on the hydrologic regime. Baseflow was estimated using the two parameter

168 recursive baseflow filter of *Eckhardt* [2005] (see equation 1), with on-line updating of baseflow

169 estimates to match low flows:

$$b_k = \frac{1}{(1 - a \cdot BFI_{max})} [(1 - BFI_{max}) \cdot a \cdot b_{k-1} + (1 - a) \cdot BFI_{max} \cdot y_k] \quad (1)$$

170 where  $b_k$  is the estimated baseflow at time  $k$ ,  $y_k$  is the total observed streamflow at time  $k$ ,  $BFI_{max}$

171 is the maximum value of the BFI (long term ratio of baseflow to total streamflow) and  $a$  is a filter

172 parameter. In this study, we adopt  $BFI_{max} = 0.5$  and  $a = 0.988$  based on manual optimization.

173

Deleted: Figure 1

Deleted: Figure 1

176 An examination of the observed streamflow and rainfall records shows that distinct changes to the  
177 hydrologic regime are evident after the mid-1990s. The annual runoff coefficient ( $\frac{\text{runoff}}{\text{rainfall}}$ ) varies  
178 between 0.4 and 0.6 prior to 1994, after which it increases to between 0.6 and 0.8 until 2004 (see  
179 [Figure 2a](#)). However, increases to annual yields are driven mostly by changes to baseflow volume.  
180 This is evident in [Figure 2a](#), which shows that the increase in the annual direct runoff coefficient  
181 ( $\frac{\text{runoff} - \text{baseflow}}{\text{rainfall}}$ ) is less than the increase in the total runoff coefficient (roughly 0.1 increase  
182 compared to 0.2 respectively). A small increase in the Annual Baseflow Index ( $\frac{\text{baseflow}}{\text{runoff}}$ ) is apparent  
183 also, from about 0.32 on average in the period 1970 to 1982 to 0.39 on average after 1994 ([Figure](#)  
184 [2b](#)). This indicates that the annual increases to baseflow volume exceed the increases to direct  
185 runoff volume. Similar changes were found by *Wang et al.* [2012] who analyzed records in the  
186 entire Da River basin which drains the largest river in the Red River catchment. The exact physical  
187 processes behind the observed increase in baseflow are not precisely known, particularly since  
188 effects of land use change from forest to cropland are not unequivocal [*Price*, 2011]. Deforestation  
189 may be associated to an increase in mean annual flow and baseflow because of lower interception  
190 and evapotranspiration rates [e.g., *Keppeler and Ziemer*, 1990]. Nevertheless, permanent forest  
191 removal may decrease baseflow because of soil compaction and lower infiltration rates [e.g.,  
192 *Zimmermann et al.*, 2006; *Bormann and Klaassen*; 2008]. Some authors also show that tillage  
193 practices, associated to forest conversion to cropland, can increase soil porosity, soil water content,  
194 and infiltration, thus ultimately contributing to baseflow formation [e.g., *Alam et al.*, 2014].

195  
196 At a seasonal time scale, it is apparent that both wet and dry season flows exhibit temporal  
197 variations. We utilized the Moving Average Shifting Horizon (MASH) [*Anghileri et al.*, 2014] and  
198 Mann-Kendall test to assess seasonal trends in observed streamflow, precipitation, and temperature  
199 data. The MASH tool can be used to qualitatively assess inter-annual variations in the seasonal  
200 pattern of a variable. It works by calculating a statistic of the data (e.g. mean) over the same block of

Deleted: Figure 2

Deleted: Figure 2

Deleted: Figure 2

204 days in consecutive years. A steady increase in baseflow is again apparent (see February to April in  
205 [Figure 2c](#)), as well as increases to wet season flows (see June to September in [Figure 2c](#)). Mann-  
206 Kendall test (with significance level equal to 5%) on annual and monthly streamflow time series  
207 shows increasing trends in almost all months, i.e., from October to July. No concurrent increases are  
208 apparent in rainfall (see [Figure 2d](#)). Also, the Mann-Kendall test applied to precipitation time series  
209 does not show any statistically significant trend, except a decrease in September for Nammuc and  
210 Quynh Nhai station and an increase in July for Dien Bien station. Temperature variations are not  
211 evident from the MASH analysis (not shown) and no significant trend can be detected by applying the  
212 Mann-Kendall test. These results indicate that changes in streamflow dynamics are likely due to land  
213 use change rather than climatic impacts.

Deleted: Figure 2

Deleted: Figure 2

Deleted: Figure 2

### 214 3. Experimental Setup

#### 215 3.1. Hydrologic Models

216 Conceptual lumped models operating at a daily time step were adopted due to the availability of  
217 point rather than distributed hydro-meteorological data of sufficient length. We considered the  
218 HyMOD [Boyle, 2001] and Hydrologiska Byrans Vattenbalansavdelning (HBV) [Bergstrom et al., 1995]  
219 models. They differ mainly in the way components of the response flow are separated (HBV has near  
220 surface flow, interflow, and baseflow components whilst HyMOD has a quickflow and slow flow  
221 component only) and how these flows are routed. A schematic of the models is shown in [Figure 3](#).

Deleted: Figure 3

222  
223 In the HyMOD model, spatial variations in catchment soil storage capacity are represented by a  
224 Pareto distribution with shape parameter  $b$  and maximum point soil storage depth  $c_{max}$ . Excess  
225 rainfall ( $V$ ) is partitioned into three cascading tanks representing quick flow and a single slow flow  
226 store through the splitting parameter  $\alpha$ . Outflow from these linear routing tanks is controlled by

231 parameters  $k_q$  (for the quick flow stores) and  $k_s$  (for the slow flow store). The model has a total of 5  
232 states and 5 parameters.

233

234 In the HBV model, input to the soil store is represented by a power-law function (see [Figure 3](#), note  
235 the snow store is neglected for this study). Excess rainfall enters a shallow layer store which  
236 generates: 1) near surface flow ( $q_0$ ) whenever the shallow store state ( $stw1$ ) is above a threshold  
237 ( $hl1$ ) and 2) interflow ( $q_1$ ) by a linear routing mechanism controlled by the  $K1$  parameter.  
238 Percolation from the shallow layer store to the deep layer store (controlled by  $perc$  parameter) then  
239 leads to the generation of baseflow also via linear routing (controlled by the  $K2$  parameter). Finally, a  
240 triangular weighting function of base length  $Maxbas$  is used to route the sum of all three flow  
241 components. There are a total of 9 parameters and 3 states.

242

243 The Shuffled Complex Evolution Algorithm (SCE-UA) [Duan *et al.*, 1993] was used to calibrate HyMOD  
244 and the Borg Evolutionary Algorithm [Hadka & Reed, 2013] was used to calibrate HBV. The  
245 calibration algorithms were selected based on previous studies that had successfully used them for  
246 calibration of these models [Reed *et al.*, 2013; Moradkhani *et al.*, 2005]. The calibration procedure  
247 itself is however not critical in our study, because the optimal parameter values are only used as  
248 initial values for the time varying parameter method. Both models were calibrated to pre-change  
249 conditions. The period 1973 to 1979 was selected for calibration (with 2 years for spin-up) as it was  
250 expected to have minimal land cover changes (and is therefore representative of pre-change  
251 conditions), and also to ensure sufficient data on pre-change conditions is available for assimilation.

252 Both models had very similar performance in terms of reproducing observed runoff (a [Nash Sutcliffe](#)  
253 [Efficiency](#) of 0.75 and 0.77 for HyMOD and HBV respectively). HBV was slightly better at reproducing  
254 low flows whilst HyMOD was slightly better at mid-range flows (see [Table 2](#)). Here the low flow  
255 threshold was defined as the average annual 50<sup>th</sup> percentile flow and the high flow threshold as the  
256 average annual 85<sup>th</sup> percentile flow.

Deleted: Figure 3

Deleted: n

Deleted: Table 2

## 260 3.2. Time Varying Parameter Estimation

261 A Data Assimilation based framework for estimating time varying parameters was presented in  
262 *Pathiraja et al.* [2016a]. The approach relies on an Ensemble Kalman Filter (EnKF) [Evensen,1994] to  
263 perform sequential joint state and parameter updating. EnKFs were developed to extend the  
264 applicability of the celebrated Kalman Filter [Kalman, 1960] to non-linear systems, although they  
265 provide a sub-optimal update as only the mean and covariance are considered in generating the  
266 posterior. However, they have been used with much success in many hydrologic applications [see for  
267 example *Reichle et al.*, 2002; *Gu et al.*, 2005; *Komma et al.*, 2008; *Sun et al.*, 2009; *Xu et al.*, 2016].  
268 EnKFs offer a practical alternative to Sequential Monte Carlo/Particle Filter methods that propagate  
269 the full probability density through time, but suffer from several implementation issues even in  
270 moderate dimensional systems. The Locally Linear Dual EnKF method of *Pathiraja et al.* [2016a]  
271 works by sequentially proposing parameters, updating these using the Ensemble Kalman filter and  
272 available observations, and subsequently using these updated parameters to propose and update  
273 model states. An approach for proposing parameters in the time varying setting was also presented,  
274 for cases where no prior knowledge of parameter variations is available. The method was verified  
275 against multiple synthetic case studies as well as for 2 small experimental catchments experiencing  
276 controlled land use change [*Pathiraja et al.*, 2016a and *Pathiraja et al.*, 2016b]. The algorithm is  
277 summarised below, for full details refer to *Pathiraja et al.* [2016a].

### 278 3.2.1. Locally Linear Dual EnKF

279 Suppose a dynamical system can be described by a vector of states  $\mathbf{x}_t$  and outputs  $\mathbf{y}_t$  and a vector of  
280 associated model parameters  $\boldsymbol{\theta}_t$  at any given time  $t$ . The uncertain system states and parameters  
281 are represented by an ensemble of states  $\{\mathbf{x}_t^i\}_{i=1:n}$  and parameters  $\{\boldsymbol{\theta}_t^i\}_{i=1:n}$  each with  $n$  members.  
282 The prior state and parameter distributions  $\{\mathbf{x}_t^{i-}\}_{i=1:n}$  and  $\{\boldsymbol{\theta}_t^{i-}\}_{i=1:n}$  respectively represent our  
283 prior knowledge of the system, usually derived as the output from a numerical model. Suppose also  
284 that the system outputs are observed ( $\mathbf{y}_t^o$ ) but that there is also some uncertainty associated with

285 these observations. The purpose of the data assimilation algorithm (here the EnKF) is to combine the  
 286 prior estimates with measurements, based on their respective uncertainties, to obtain an improved  
 287 estimate of the system states and parameters. A single cycle of the Locally Linear Dual EnKF  
 288 procedure for a given time  $t$  is undertaken as follows. Note in the following, the overbar notation is  
 289 used to indicate the ensemble mean.

290

291 1. **Propose a prior parameter ensemble.** This involves generating a parameter ensemble using  
 292 prior knowledge. In this case, our prior knowledge comes from the updated parameter  
 293 ensemble from the previous time ( $\theta_{t-1}^{i+}$ ) and how it has changed over recent time steps. The  
 294 assumed parameter dynamics is a Gaussian random walk with time varying mean and  
 295 variance, given by:

$$\theta_t^{i-} \sim N(\theta_{t-1}^{i+} + \mathbf{m}_t \cdot \Delta t, s^2 \Sigma_{t-1}^\theta) \text{ for } i = 1:n \quad (2)$$

$$\Sigma_{t-1}^\theta = \frac{1}{n-1} \sum_{i=1}^n (\theta_{t-1}^{i+} - \overline{\theta_{t-1}^+}) (\theta_{t-1}^{i+} - \overline{\theta_{t-1}^+})^T \quad (3)$$

296 where  $\Sigma_{t-1}^\theta$  is the sample covariance matrix of the updated parameter ensemble at time  $t -$   
 297 1;  $\overline{\theta_{t-1}^+}$  indicates the ensemble mean of the updated parameters at time  $t - 1$ ;  $()^T$   
 298 represents the transpose operator; and  $s^2$  is a tuning parameter. The prior ensemble mean  
 299 is determined as the linear extrapolation of the updated ensemble means from the previous  
 300 two time steps, i.e.:

$$\mathbf{m}_t[k] = \begin{cases} \mathbf{m}_{t-1}[k], & |\mathbf{m}_{t-1}[k]| \leq m_{max} \\ \mathbf{m}_{t-2}[k], & |\mathbf{m}_{t-1}[k]| > m_{max} \end{cases} \quad (4)$$

$$\mathbf{m}_{t-1} = \frac{\overline{\theta_{t-1}^+} - \overline{\theta_{t-2}^+}}{\Delta t} \quad (5)$$

$$\mathbf{m}_{t-2} = \frac{\overline{\theta_{t-2}^+} - \overline{\theta_{t-3}^+}}{\Delta t} \quad (6)$$

301 where  $\mathbf{m}_t[k]$  indicates the  $k$ th component of the vector  $\mathbf{m}_t$ , the estimated rate of change.

302 Note that the extrapolation is forced to be less than a pre-defined maximum rate of change

303  $m_{max}$  to minimise overfitting and avoid parameter drift due to isolated large updates. The

304 maximum rate of change is model specific and will depend on the modeller's judgement  
 305 regarding expected extreme changes.

306 2. **Consider observation and forcing uncertainty.** This is done by perturbing measurements of  
 307 forcings and system outputs with random noise sampled from a distribution representing the  
 308 uncertainty in those measurements. The result is an ensemble of forcings ( $\mathbf{u}_t^i$ ) and  
 309 observations ( $\mathbf{y}_t^i$ ) each with  $n$  members. For example, if random errors in measurements of  
 310 system outputs (herein also referred as observations) are characterized by a zero mean  
 311 Gaussian distribution, the ensemble of observations is given by:

$$\mathbf{y}_t^i \sim N(\mathbf{y}_t^o, \Sigma_t^{y^o y^o}) \text{ for } i = 1:n \quad (7)$$

312 where  $\mathbf{y}_t^o$  is the recorded measurement at time  $t$  and  $\Sigma_t^{y^o y^o}$  is the error covariance matrix of  
 313 the measurements.

314 3. **Generate simulations using prior parameters.** The prior parameters from Step 1,  $\theta_t^{i-}$  and  
 315 updated states from the previous time,  $\mathbf{x}_{t-1}^{i+}$  are forced through the model equations to  
 316 generate an ensemble of model simulations of states ( $\hat{\mathbf{x}}_t^i$ ) and outputs ( $\hat{\mathbf{y}}_t^i$ ):

$$\hat{\mathbf{x}}_t^i = f(\mathbf{x}_{t-1}^{i+}, \theta_t^{i-}, \mathbf{u}_t^i) \text{ for } i = 1:n \quad (8)$$

$$\hat{\mathbf{y}}_t^i = h(\hat{\mathbf{x}}_t^i, \theta_t^{i-}) \text{ for } i = 1:n \quad (9)$$

317 4. **Perform the Kalman update of parameters.** Parameters are updated using the Kalman  
 318 update equation and the prior parameter and simulated output ensemble from Step 1 and 3:

$$\theta_t^{i+} = \theta_t^{i-} + \mathbf{K}_t^\theta (\mathbf{y}_t^i - \hat{\mathbf{y}}_t^i) \text{ for } i = 1:n \quad (10)$$

$$\mathbf{K}_t^\theta = \Sigma_t^{\theta \hat{\mathbf{y}}} [\Sigma_t^{\hat{\mathbf{y}} \hat{\mathbf{y}}} + \Sigma_t^{y^o y^o}]^{-1} \quad (11)$$

319 where  $\Sigma_t^{\theta \hat{\mathbf{y}}}$  is a matrix of the sample cross covariance between errors in parameters  $\theta_t^{i-}$  and  
 320 simulated output  $\hat{\mathbf{y}}_t^i$ ; and  $\Sigma_t^{\hat{\mathbf{y}} \hat{\mathbf{y}}}$  is the sample error covariance matrix of the simulated output:

$$\Sigma_t^{\theta \hat{\mathbf{y}}} = \frac{1}{n-1} \sum_{i=1}^n (\theta_t^{i-} - \bar{\theta}_t) (\hat{\mathbf{y}}_t^i - \bar{\hat{\mathbf{y}}}_t)^\top \quad (12)$$

$$\Sigma_t^{\hat{\mathbf{y}} \hat{\mathbf{y}}} = \frac{1}{n-1} \sum_{i=1}^n (\hat{\mathbf{y}}_t^i - \bar{\hat{\mathbf{y}}}_t) (\hat{\mathbf{y}}_t^i - \bar{\hat{\mathbf{y}}}_t)^\top \quad (13)$$

321 5. **Generate simulations using updated parameters.** Step 3 is repeated with the updated  
 322 parameter ensemble  $\theta_t^{i+}$  to generate the prior ensemble of model simulations of states ( $x_t^{i-}$ )  
 323 and outputs ( $\tilde{y}_t^i$ ):

$$x_t^{i-} = f(x_{t-1}^{i+}, \theta_t^{i+}, u_t^i) \text{ for } i = 1:n \quad (14)$$

$$\tilde{y}_t^i = h(x_t^{i-}, \theta_t^{i+}) \text{ for } i = 1:n \quad (15)$$

324 6. **Perform the Kalman update of states and outputs.** Use the Kalman update equation for  
 325 correlated measurement and process noise (equations 16 to 19) and the simulated state  
 326 ( $x_t^{i-}$ ) and output ( $\tilde{y}_t^i$ ) ensembles from Step 5 to update them. Since the measurements have  
 327 already been used to generate  $\tilde{y}_t^i$ , the errors in model simulations and measurements are  
 328 now correlated. The standard Kalman update equation (as in the form of equations 10 and  
 329 11) can no longer be used as it relies on the assumption that errors in measurements and  
 330 model simulations are independent.

$$x_t^{i+} = x_t^{i-} + K_t^x (y_t^i - \tilde{y}_t^i) \text{ for } i = 1:n \quad (16)$$

$$K_t^x = [\Sigma_t^{xy} + \Sigma_t^{xy^o}] [\Sigma_t^{yy} + \Sigma_t^{xy^o} + (\Sigma_t^{xy^o})^T + \Sigma_t^{y^o y^o}]^{-1} \quad (17)$$

$$\epsilon_{x_t}^i = x_t^{i-} - \hat{x}_t^i \quad (18)$$

$$\epsilon_{y_t}^i = \tilde{y}_t^i - \hat{y}_t^i \quad (19)$$

331 where  $\Sigma_t^{xy}$  is a matrix of the sample cross covariance between simulated states  $\{x_t^{i-}\}_{i=1:n}$   
 332 and outputs  $\{\tilde{y}_t^i\}_{i=1:n}$  from Step 5;  $\Sigma_t^{xy^o}$  represents the sample covariance between  
 333  $\{\epsilon_{x_t}^i\}_{i=1:n}$  and the observations; and  $\Sigma_t^{y^o y^o}$  represents the sample covariance between the  
 334  $\{\epsilon_{y_t}^i\}_{i=1:n}$  and the observations.

335 The above algorithm specifies the updating of states and parameters at any given time, based on  
 336 available observations. This allows one to retrospectively estimate time variations in model  
 337 parameters, as well as provide one time step ahead forecasts of states & outputs (as per equations 8  
 338 and 9). Forecasts at longer time horizons (i.e. longer than one time step ahead) would be made by

Deleted: 15

Deleted: 18

Deleted: 10

Deleted: 11

Deleted: 8

Deleted: 9

345 generating prior parameters and states as detailed in Steps 1 to 3, although the local linear  
346 extrapolations are only valid close to the current time point.

### 347 3.2.2. Application to the Nammuc Catchment

348 Joint state and parameter estimation was undertaken for the Nammuc Catchment over the period  
349 1980 to 2004 by assimilating streamflow observations into the HyMOD and HBV models at a daily  
350 time step. Additionally, simulations using the time invariant parameters obtained from calibration

351 over the period 1973-1979 were generated for 1980 to 2004, for comparison. Estimating a large  
352 number of parameters from limited data is problematic in that the system is highly under-

353 determined, making it difficult to ensure the estimated parameters are meaningful. Given the fairly

354 low parameter dimensionality of HyMOD, all model parameters were allowed to vary in time whilst

355 for HBV we applied the Sobol method to identify the most sensitive parameters to be included in the

356 time varying parameter estimation. The Sobol method is a global sensitivity analysis method based

357 on variance decomposition. It identifies the partial variance contribution of each parameter to the

358 total variance of the hydrological model output [see for example *Saltelli et al., 2008, Nossent et al.*

359 *2011*]. The method, implemented through the SAFE toolbox [*Pianosi et al., 2015*], found the *lp* and

360 *Maxbas* parameters to be the least sensitive and least important in defining variations to catchment

361 hydrology (see Table 3). These were held fixed (*lp* = 1 and *Maxbas* = 1 day) in the following analysis.

362 Note that although the *hl1* parameter was found to have low sensitivity, it was retained as a time

363 varying parameter due to its conceptual importance in separating interflow and near surface flow

364 (refer [Figure 3](#)).

365

366 Unbiased normally distributed ensembles of the parameters and states are required to initialise the

367 LL Dual EnKF. Initial parameter ensembles were generated by sampling from a Gaussian distribution

368 with mean equal to the calibrated parameters over the pre-change period and variance estimated

369 from parameter sets with similar objective function values. Parameter sets with similar objective

Deleted:

Deleted:

Deleted: Figure 3

373 function values were obtained when using different starting points to the optimization algorithm  
374 during the model calibration stage. Initial state ensembles were also sampled from normal  
375 distributions with mean equal to the simulated state at the end of the calibration period. An  
376 ensemble size of 100 members was adopted and assumed sufficiently large based on the findings of  
377 *Moradkhani et al.* [2005] and *Aksoy et al.* [2006]. Due to the stochastic-dynamic nature of the  
378 method, ensemble statistics were calculated over 20 separate realisations of the LL Dual EnKF. The  
379 prior parameter generating method described in Step 1 of Section 3.2 requires specification of the  
380 tuning parameter  $s^2$  to define the variance of the perturbations. This was tuned by selecting the  $s^2$   
381 value that optimized the quality of forecast streamflow over the calibration period. Forecast quality  
382 was assessed using the logarithmic score (LS) [*Good, 1952*] of background streamflow predictions  
383 ( $\tilde{y}_t^i$ ) using updated parameters (equation 15), which was averaged over the calibration period of  
384 length  $T$ :

$$\overline{LS} = \sum_{t=1}^T LS_t \quad (20)$$

$$LS_t = \log (f(y = y_t^o)) \quad (21)$$

385 where  $f(y)$  is the probability density function of the background streamflow predictions  
386 (represented by the empirical pdf of the sample points  $\{\tilde{y}_t^i\}_{i=1:n}$ ); and  $y_t^o$  is the measurement of the  
387 system outputs. The  $s^2$  value that gave the largest  $\overline{LS}$  was adopted for the assimilation period. The  
388 maximum allowable daily rate of change in the ensemble mean was based on assuming a linear rate  
389 of change within the entire feasible parameter space over a three year period.

390  
391 As detailed in Section 3.2, observation and forcing uncertainty is considered by perturbing  
392 measurements with random noise. Here streamflow errors were assumed to be zero-mean normally  
393 distributed (truncated to ensure positivity) and heteroscedastic. The variance is defined as a  
394 proportion of the observed streamflow, to reflect the fact that larger flows tend to have greater  
395 errors than low flows:

Deleted: 15

$$y_t^i \sim TN(y_t^0, d, y_t^0) \text{ for } i = 1:n \quad (22)$$

397 where TN indicates the truncated normal distribution to ensure positive flows and  $d = 0.1$ . A  
 398 multiplier of 0.1 was chosen based on estimates adopted for similar gauges in hydrologic DA studies  
 399 [e.g. Clark *et al.*, 2008; Weerts & Serafy, 2006; Xie *et al.*, 2014].

400  
 401 Several studies have noted that a major source of rainfall uncertainty arises from scaling point  
 402 rainfall to the catchment scale [Villarini & Krajewski, 2008; McMillan *et al.*, 2011] and that  
 403 multiplicative errors models are suited to describing such errors [e.g. Kavetski *et al.*, 2006]. Rainfall  
 404 uncertainties were therefore described using unbiased, lognormally distributed multipliers:

$$P_t^i = P_t \cdot M^i \quad (23)$$

$$M^i \sim LN(m, v) \text{ and } X^i = \log(M^i) \sim N(\mu, \sigma^2) \text{ for } i = 1:n \quad (24)$$

405 where  $P_t$  is the measured rainfall at time  $t$ ;  $m$  and  $v$  are the mean and variance of the lognormally  
 406 distributed rainfall multipliers  $M$  respectively; and  $\mu$  and  $\sigma^2$  are the mean and variance of the  
 407 normally distributed logarithm of the rainfall multipliers  $M$ . For unbiased perturbations, we let  $m =$   
 408 1. The variance of the rainfall multipliers ( $v$ ) was estimated by considering upper and lower bound  
 409 error estimates in the Thiessen weights assigned to the four rainfall stations (see Section 2.1 for  
 410 calculation of catchment averaged rainfall,  $P_t$ ). The resulting upper and lower bound catchment  
 411 averaged rainfall data were then used to estimate error parameters due to spatial variation in  
 412 rainfall:

$$v = e^{(2\mu + \sigma^2)} \cdot (e^{\sigma^2} - 1) \quad (25)$$

$$\sigma^2 = \widehat{\sigma^2} = \text{var} \left( \log \left[ \frac{P_{upper,10}}{P_{lower,10}} \right] \right) \quad (26)$$

$$\mu = \log(m) - \frac{\sigma^2}{2} = -\frac{\sigma^2}{2} \quad (27)$$

413 where  $P_{upper,10}$  indicates catchment averaged rainfall data estimated using the upper bound  
 414 Thiessen weights with daily depth greater than 10mm (similar for  $P_{lower,10}$ ). A 10mm rainfall depth  
 415 threshold was chosen to avoid large rainfall fractions due to small rainfall depths.  $\widehat{\sigma^2}$  was found to

416 be 0.05 in this case study. Similarly, we assume the dominant source of uncertainty in temperature  
417 data arises from spatial variation. Differences in temperature records at Lai Chau and Quynh Nhai  
418 (only available gauges with temperature records) were analysed and found to be approximately  
419 normally distributed with sample mean 0.2 deg C and variance of 1.4 deg C. A perturbed  
420 temperature ensemble was then generated according to equation 28;

$$T_t^i \sim TN(T_t^{avg}, 1.4) \text{ for } i = 1:n \quad (28)$$

421 where  $T_t^{avg}$  represents catchment averaged temperature data (see Section 2.1). Note that  
422 perturbations were taken to be unbiased (zero mean) as the sample mean of the differences in the  
423 temperature records was close to zero. The same perturbed input and observation sequences were  
424 used for the HyMOD and HBV runs for the sake of comparison. A summary of the values adopted for  
425 the various components of the Locally Linear Dual EnKF for each model is provided in [Table 4](#) and  
426 [Table 5](#).

## 427 4. Results and Discussion

428 Temporal variations in the estimated parameter distributions from the LL Dual EnKF are evident for  
429 both models (see Figure 4 and 5). In the case of the HBV model, changes at an inter-annual time  
430 scale are evident for the  $perc$  and  $\beta$  (see [Figure 4](#)). The decrease in the  $\beta$  parameter means that a  
431 greater proportion of rainfall is converted to runoff (i.e. more water entering the shallow layer  
432 storage). Additionally, the increase in the  $perc$  parameter means that a greater volume of water is  
433 made available for baseflow generation. These changes correspond with the observed increase in  
434 the annual runoff coefficient ([Figure 2](#)) and increase in baseflow volume (as discussed in Section 2.2).  
435 From an algorithm perspective, these parameters are most strongly correlated with streamflow (as  
436 well as the most sensitive, see Table 3), meaning that they will receive the greatest proportional  
437 updates. Similar parameter adjustments are seen for HyMOD, at least at a qualitative level (see  
438 [Figure 5](#)). The sharp increase in the  $b$  parameter during the post-change period means that a greater

Deleted: 27

Deleted: Table 4

Deleted: Table 5

Deleted: Figure 4

Deleted: Figure 2

Deleted: Figure 5

445 volume of water is available for routing (as larger  $b$  values mean that a smaller proportion of the  
446 catchment has deep soil storage capacity) and the downward inter-annual trend in  $\alpha$  means that a  
447 greater portion of excess runoff is routed through the baseflow store. Intra-annual variations in  
448 updated model parameters for both HyMOD and HBV are also apparent (refer [Figure 4](#) and [Figure 5](#)).  
449 This is due to the inability of a single parameter distribution to accurately model both wet and dry  
450 season flows. Such variations were not observed when using the time varying parameter framework  
451 for small deforested catchments (< 350ha) [see *Pathiraja et al.*, 2016b]. The comparatively less clear  
452 parameter changes for the Nammuc catchment are due to a combination of the increased difficulty  
453 in accurately modelling the hydrologic response (even in pre-change conditions) and due to the  
454 relatively more subtle and gradual changes to land cover. Nonetheless, the method is shown to  
455 generate a temporally varying structure that is conceptually representative of the observed changes.  
456  
457 Despite the overall correspondence between changes to model parameters and observed  
458 streamflow, a closer examination shows that the hydrologic model structure is critical in determining  
459 whether the time varying parameter models accurately reflect changes in all aspects of the  
460 hydrologic response (not just total streamflow). In order to examine the impact of parameter  
461 variations on the model dynamics, we generated model simulations with the time varying parameter  
462 ensemble from the LL Dual EnKF, but without state updating (hereafter referred to as TVP-HBV and  
463 TVP-HyMOD). Streamflow predictions from the LL Dual EnKF (i.e. with state and parameter updating)  
464 for both the HyMOD and HBV are generally of similar quality and superior to those from the  
465 respective time invariant parameter models [that have been calibrated on pre-change data \(1975-](#)  
466 [1979\)](#), although a slight bias in baseflow predictions from HyMOD is evident (see for example [Figure](#)  
467 [6](#)). [The Nash Sutcliffe Efficiency of one step ahead streamflow predictions over the period 1980 –](#)  
468 [2004 from the LL Dual EnKF is 0.87 when using HyMOD or HBV, compared to 0.76 and 0.72 for the](#)  
469 [respective time invariant parameter models evaluated over the same period.](#) However, differences  
470 in predictions from TVP-HBV and TVP-HyMOD are more striking due to the lack of state updating.

Deleted: Figure 4

Deleted: Figure 5

Deleted: OD

Deleted: Figure 6

475 [Figure 7](#) shows annual statistics of simulated streamflow from the TVP-HBV and TVP-HyMOD models  
476 and observed runoff. The TVP-HBV gives direct runoff and baseflow predictions that are consistent  
477 with runoff observations, meaning that the parameter adjustments reflect the observed changes in  
478 the runoff response. This however is not the case for the TVP-HyMOD. The annual runoff coefficient  
479 and annual direct runoff coefficient are severely under-estimated in the post-change period by the  
480 TVP-HyMOD, whilst the Annual Baseflow Index has an increasing trend of magnitude far greater than  
481 observed ([Figure 7c](#)). All three quantities on the other hand are well represented by the TVP-HBV  
482 ([Figure 7](#)). Similar conclusions can be drawn from [Figure 8](#), which shows the results of a Moving  
483 Average Shifting Horizon (MASH) analysis (see Section 2.2) on total and direct runoff (observed and  
484 simulated). Observed increases in January to April flows (see [Figure 8a](#)) and wet season direct flows  
485 (July to September) (see [Figure 8e](#)) are well represented by the TVP-HBV but not TVP-HyMOD.  
486  
487 The reason for the differences in performance between the TVP-HBV and TVP-HyMOD lies in the  
488 structure of the hydrologic model. The TVP-HyMOD is incapable of representing the observed  
489 increase in annual runoff/direct runoff coefficient due to the increased baseflow during dry periods,  
490 despite having an Annual Baseflow Index far greater than the observed. This occurs due to an  
491 inability to generate flow volume during periods of no rain. In joint state-parameter updating using  
492 HyMOD, underestimated runoff predictions during dry periods lead to adjustments to the  $k_s$  and  $\alpha$   
493 parameters to increase baseflow depth (since these are the only parameters that are associated to  
494 an active store). Unlike HBV, HyMOD has no continuous supply of water to the routing stores (i.e.  
495 the quick flow and slow flow stores) during recession periods (which typically have extended periods  
496 of no rainfall, so that  $V$  in [Figure 3](#) is zero). This means that  $k_s$  and  $\alpha$  are updated to extreme values  
497 to compensate for the volumetric shortfall. The HBV structure, on the other hand, has a continuous  
498 percolation of water into the deep layer store even during periods of no rain (so long as the shallow  
499 water store is non-empty). In summary, the HyMOD model structure is poorly suited to simulating  
500 streamflow dynamics in post-change conditions, although it gave reasonable simulations in pre-

Deleted: Figure 7

Deleted: Figure 7

Deleted: Figure 7

Deleted: Figure 8

Deleted: Figure 8

Deleted: Figure 8

Deleted: Figure 3

508 change conditions. This highlights that need to select a sufficiently flexible model structure prior to  
509 undertaking forecasting/predictive modelling using the time varying parameter approach. In  
510 particular, the model structure must be capable of effectively simulating all potential future  
511 catchment conditions.

512  
513 Having established that the TVP-HBV provided a good representation of the observed streamflow  
514 dynamics, we used a modelling approach to determine whether the observed changes were solely  
515 driven by forcings and which (if any) components of runoff were also affected by land use change. A  
516 resampled rainfall and temperature time series was generated by sampling the data without  
517 replacement across years for each day (for instance rainfall and temperature for 1<sup>st</sup> January 1990 is  
518 found by randomly sampling from all records on 1<sup>st</sup> January). This maintains the intra-annual (e.g.  
519 seasonal) variability but destroys any inter-annual trends in the meteorological data. Streamflow  
520 simulations were then generated using this resampled meteorological sequence as inputs to the TVP-  
521 HBV (i.e. without state updating). If the resulting streamflow simulations do not reproduce the  
522 observed changes to streamflow dynamics, then this indicates that changes to meteorological  
523 forcings are the main contributor. However, if it is able to at least partially (or fully) reproduce the  
524 observed streamflow changes, this means that land cover changes are impacting catchment  
525 hydrology (but potentially in addition to forcing changes, due to the presence of ecosystem

526 feedbacks). [Figure 8d&h](#) show the results of a MASH undertaken on the resulting simulations of total  
527 and direct runoff using the resampled forcing time series and TVP-HBV model. Observed increases in  
528 baseflow during the January – April period (see [Figure 8a](#)) and increases in direct runoff in the June –  
529 September period (see [Figure 8e](#)) are reproduced. The magnitude of increase in direct runoff in July  
530 is slightly lower, indicating the potential for some climatic influences also. This is consistent with  
531 findings from the Mann-Kendall test which identified a statistically significant increase in July rainfall  
532 (see Section 2.2). Overall however, these results lend further weight to the conclusion that land  
533 cover change has impacted the hydrologic regime of the Nammuc catchment. These results also

Deleted: Figure 8

Deleted: Figure 8

Deleted: Figure 8

537 demonstrate that parameter changes correspond to actual changes in catchment hydrology, and are  
538 not just random fluctuations that reproduce the observed streamflow statistics only when the  
539 observed forcing time series is used.

## 540 **5. Conclusions**

541 As our anthropogenic footprint expands, it will become increasingly important to develop modelling  
542 methodologies that are capable of handling changing catchment conditions. Previous work proposed  
543 the use of models whose parameters vary with time in response to signals of change in observations.  
544 The so-called Locally Linear Dual EnKF time varying parameter estimation algorithm [*Pathiraja et al.,*  
545 2016a] was applied to 2 sets of small (< 350 ha) paired experimental catchments with deforestation  
546 occurring under experimental conditions (rapid clearing of 100% and 50% of land surface) [*Pathiraja*  
547 *et al., 2016b*]. Here we demonstrate the efficacy of the method for a larger catchment experiencing  
548 more realistic land cover change, whilst also investigating the importance of the chosen model  
549 structure in ensuring the success of the time varying parameter estimation method. We also  
550 demonstrate that the time varying parameter framework can be used in a retrospective fashion to  
551 determine whether land cover changes (and not just meteorological factors) contribute to the  
552 observed hydrologic changes.

553

554 Experiments were undertaken on the Nammuc catchment (2880 km<sup>2</sup>) in Vietnam, which experienced  
555 a relatively gradual conversion from forest to cropland over a number of years (cropland increased  
556 from roughly 23% of the catchment between 1981 and 1994 to 52% by 2000). Changes to the  
557 hydrologic regime after the mid-1990s were detected and attributed mostly to an increase in  
558 baseflow volume. Application of the LL Dual EnKF with two conceptual models (HBV and HyMOD)  
559 showed that the time varying parameter framework with state updating improved streamflow  
560 prediction in post-change conditions compared to the time invariant parameter case. However,  
561 baseflow predictions from the LL Dual EnKF with HBV were generally superior to the HyMOD case

562 which tended to have a slight negative bias. It was found that the structure (i.e. model equations) of  
563 HyMOD was unsuited to representing the modified baseflow conditions, resulting in extreme and  
564 unrealistic time varying parameter estimates. This work shows that the chosen model is critical for  
565 ensuring the time varying parameter framework successfully models streamflow in unknown future  
566 land cover conditions, particularly when used in a real time forecasting mode. Appropriate model  
567 selection can be a difficult task due to the significant uncertainty associated with future land use  
568 change, and can be even more problematic when multiple models have similar performance in pre-  
569 change conditions (as was the case in this study). One possible way to ensure success of the time  
570 varying parameter approach is to use models whose fundamental equations explicitly represent key  
571 physical processes (for instance, modelling sub-surface flow using Richard's equation with hydraulic  
572 conductivity allowed to vary with time). In this way, time variations in model parameters would  
573 more closely reflect changes to physiographic properties, rather than also having to account for  
574 missing processes. The drawback of such physically based models is that they are generally data  
575 intensive, both in generating model simulations (i.e. detailed inputs) and specifying parameters.  
576 Additionally, it may be necessary to reduce the dimensionality of the time varying parameter vector  
577 by keeping less sensitive model parameters fixed in order to make the estimation problem tractable.  
578 Models of intermediate complexity that have explicit process descriptions may be the most  
579 promising, although this also remains to be demonstrated.

## 580 **6. Acknowledgements**

581 This study was funded by the Australian Research Council as part of the Discovery Project  
582 DP140102394. Dr. Marshall is additionally supported through a Future Fellowship FT120100269. [The](#)  
583 [research of Dr. Pathiraja has been partially funded by Deutsche Forschungsgemeinschaft \(DFG\)](#)  
584 [through the grant CRC 1294 "Data Assimilation."](#)  
585

586 The data used in this paper were collected under the project IMRR (Integrated and sustainable water  
587 Management of Red Thai Binh Rivers System in changing climate), funded by the Italian Ministry of  
588 Foreign Affairs (Delibera n. 142 del 8 Novembre 2010). We greatly acknowledge Dr. Andrea  
589 Castelletti for provision of data and for discussions on this work.  
590  
591 Data utilized in this study can be made available from the authors upon request.

## 592 7. References

- 593 Aksoy, A., Zhang, F., Nielsen-Gammon, J. (2006). Ensemble-Based Simultaneous State and Parameter  
594 Estimation in a Two-Dimensional Sea-Breeze Model. *Monthly Weather Review*, 134, 2951–2970.  
595
- 596 Alam, M., Islam, M., Salahin, N., and Hasanuzzaman, M. (2014) Effect of tillage practices on soil  
597 properties and crop productivity in wheat-mungbean-rice cropping system under subtropical  
598 climatic conditions. *The Scientific World Journal* 2014,  
599 <https://www.hindawi.com/journals/tswj/2014/437283/>
- 600 Anghileri, D., Pianosi, F., & Soncini-Sessa, R. (2014). Trend detection in seasonal data: From hydrology  
601 to water resources. *Journal of Hydrology*, 511, 171–179.  
602 <http://doi.org/10.1016/j.jhydrol.2014.01.022>
- 603 Bergström, S. 1995. The HBV model. In: Singh, V.P. (Ed.) *Computer Models of Watershed Hydrology*.  
604 Water Resources Publications, Highlands Ranch, CO., pp. 443-476.
- 605 Bhaduri, B. B., Minner, M., Tatalovich, S., Member, A., & Harbor, J. (2001). Long-term hydrologic  
606 impact of urbanization: A tale of two models. *Journal of Water Resources Planning and*  
607 *Management*, 127(February), 13–19.
- 608 Bormann, H., and K. Klaassen (2008) Seasonal and land use dependent variability of soil hydraulic and  
609 soil hydrological properties of two Northern German soils. *Geoderma* 145.3-4 (2008): 295-302.  
610 <https://www.sciencedirect.com/science/article/pii/S0016706108000918#bib6>
- 611 Boyle, D. (2001). Multicriteria calibration of hydrological models, *Ph.D. dissertation*, Univ. of Ariz.,  
612 Tucson.
- 613 Brown, A. E., McMahon, T. A., Podger, G. M., & Zhang, L. (2006). A methodology to predict the impact  
614 of changes in forest cover on flow duration curves, *CSIRO Land and Water Science Report 8/06*.
- 615 Brown, A. E., Western, A. W., McMahon, T. a., & Zhang, L. (2013). Impact of forest cover changes on  
616 annual streamflow and flow duration curves. *Journal of Hydrology*, 483, 39–50.  
617 <http://doi.org/10.1016/j.jhydrol.2012.12.031>
- 618 Clark, M. P., Rupp, D. E., Woods, R. A., Zheng, X., Ibbitt, R. P., Slater, A. G., ... Uddstrom, M. J. (2008).  
619 Hydrological data assimilation with the ensemble Kalman filter: Use of streamflow observations  
620 to update states in a distributed hydrological model. *Advances in Water Resources*, 31(10),  
621 1309–1324. <http://doi.org/10.1016/j.advwatres.2008.06.005>
- 622 Coe, M. T., Latrubesse, E. M., Ferreira, M. E., & Amsler, M. L. (2011). The effects of deforestation and  
623 climate variability on the streamflow of the Araguaia River, Brazil. *Biogeochemistry*, 105(1–3),  
624 119–131. <http://doi.org/10.1007/s10533-011-9582-2>
- 625 Coron, L., Andréassian, V., Perrin, C., Lerat, J., Vaze, J., Bourqui, M., & Hendrickx, F. (2012). Crash  
626 testing hydrological models in contrasted climate conditions: An experiment on 216 Australian  
627 catchments. *Water Resources Research*, 48(5), 1–17. <http://doi.org/10.1029/2011WR011721>

- 628 Costa, M. H., Botta, A., & Cardille, J. A. (2003). Effects of large-scale changes in land cover on the  
629 discharge of the Tocantins River, Southeastern Amazonia. *Journal of Hydrology*, 283(1–4), 206–  
630 217. [http://doi.org/10.1016/S0022-1694\(03\)00267-1](http://doi.org/10.1016/S0022-1694(03)00267-1)
- 631 Duan, Q. Y., Gupta, V. K., & Sorooshian, S. (1993). Shuffled complex evolution approach for effective  
632 and efficient global minimization. *Journal of Optimization Theory and Applications*, 76(3), 501–  
633 521. <http://doi.org/10.1007/BF00939380>
- 634 Dwarakish, G. S., & Ganasri, B. P. (2015). Impact of land use change on hydrological systems: A  
635 review of current modeling approaches. *Cogent Geoscience*, 1(1), 1115691–1115691.  
636 <http://doi.org/10.1080/23312041.2015.1115691>
- 637 Eckhardt, K. (2005). How to construct recursive digital filters for baseflow separation. *Hydrological  
638 Processes*, 19(2), 507–515. <http://doi.org/10.1002/hyp.5675>
- 639 Efstratiadis, A., Nalbantis, I., & Koutsoyiannis, D. (2015). Hydrological modelling of temporally-varying  
640 catchments: facets of change and the value of information. *Hydrological Sciences Journal*, 60(7–  
641 8), 1438–1461. <http://doi.org/10.1080/02626667.2014.982123>
- 642 Elfert, S., & Bormann, H. (2010). Simulated impact of past and possible future land use changes on  
643 the hydrological response of the Northern German lowland “Hunte” catchment. *Journal of  
644 Hydrology*, 383, 245–255. <http://dx.doi.org/10.1016/j.jhydrol.2009.12.040>
- 645 Evensen, G. (1994). Sequential data assimilation with a nonlinear quasi-geostrophic model using  
646 Monte Carlo methods to forecast error statistics. *Journal of Geophysical Research*, 99(C5).  
647 <http://doi.org/10.1029/94JC00572>
- 648 FAO (2005). Global Forest Resources Assessment 2005 (FRA 2005)
- 649 Good, I.J. (1952). Rational Decisions. *Journal of the Royal Statistical Society*. B 14: 107–114.  
650
- 651 Gu, Y., and D. S. Oliver (2005), History matching of the PUNQ-S3 reservoir model using the ensemble  
652 Kalman filter, *SPE J.*, 10(2), 217–224, <http://doi.org/10.2118/89942-PA>.  
653
- 654 Giuliani, M., Anghileri, D., Castelletti, A., Vu, P. N., & Soncini-Sessa, R. (2016). Large storage  
655 operations under climate change: expanding uncertainties and evolving tradeoffs.  
656 *Environmental Research Letters*, 11(3), 035009.  
657
- 658 Hadka, D., Reed, P., (2013). Borg: an auto-adaptive many-objective evolutionary computing  
659 framework. *Evol. Comput.* 21 (2), 231–259.
- 660 Hamon, W. (1961). Estimating potential evapotranspiration. *Transactions of the American Society of  
661 Civil Engineers*, 128(1), pp.324-337.
- 662 Kalman, R.E. (1960) A new approach to linear filtering and prediction problems, Transactions of the  
663 ASME – *Journal of Basic Engineering*, Series D, 82 (1960), 35–45.
- 664 Kavetski, D., Kuczera, G., & Franks, S. W. (2006). Bayesian analysis of input uncertainty in hydrological  
665 modeling: 1. Theory. *Water Resources Research*, 42(3), <http://doi.org/10.1029/2005WR004368>  
666

- 667 Keppeler, E. T., and R. R. Ziemer (1990) Logging effects on streamflow: water yield and summer low  
668 flows at Caspar Creek in northwestern California. *Water Resources Research* 26.7 (1990): 1669-  
669 1679.  
670 <http://onlinelibrary.wiley.com/doi/10.1029/WR026i007p01669/full>  
671
- 672 Kim, D.-H., J. O. Sexton, and J. R. Townshend (2015). Accelerated deforestation in the humid tropics  
673 from the 1990s to the 2000s, *Geophysical Research Letters*, 42, 3495–3501,  
674 <http://doi.org/10.1002/2014GL062777>.
- 675 Komma, J., G. Blöschl, and C. Reszler (2008), Soil moisture updating by Ensemble Kalman Filtering in  
676 real-time flood forecasting, *J. Hydrol.*, 357(3–4), 228–242,  
677 <http://doi.org/10.1016/j.jhydrol.2008.05.020>.  
678
- 679 Kummer, D., and Turner, B. (1994). The Human Causes of Deforestation in Southeast Asia. *BioScience*,  
680 44(5), 323-328. <http://doi.org/10.2307/1312382>  
681
- 682 Legesse, D., Vallet-Coulomb, C., & Gasse, F. (2003). Hydrological response of a catchment to climate  
683 and land-use changes in Tropical Africa: case study South Central Ethiopia. *Journal of Hydrology*,  
684 275(1-2), 67–85. [http://doi.org/10.1016/S0022-1694\(03\)00019-2](http://doi.org/10.1016/S0022-1694(03)00019-2)  
685
- 686 Marshall, L., Sharma, A. and Nott, D. (2006) 'Modeling the catchment via mixtures: Issues of model  
687 specification and validation', *Water Resources Research*, 42(11), pp. 1–14. [http://doi.org/](http://doi.org/10.1029/2005WR004613)  
688 [10.1029/2005WR004613](http://doi.org/10.1029/2005WR004613).  
689
- 690 McIntyre, N., & Marshall, M. (2010). Identification of rural land management signals in runoff  
691 response. *Hydrological Processes*, 24(24), 3521–3534. <http://doi.org/10.1002/hyp.7774>  
692
- 693 McMillan, H., Jackson, B., Clark, M., Kavetski, D., & Woods, R. (2011). Rainfall uncertainty in  
694 hydrological modelling: An evaluation of multiplicative error models. *Journal of Hydrology*,  
695 400(1-2), 83–94. <http://doi.org/10.1016/j.jhydrol.2011.01.026>
- 696 Moradkhani, H., Sorooshian, S., Gupta, H. V., & Houser, P. R. (2005). Dual state–parameter  
697 estimation of hydrological models using ensemble Kalman filter. *Advances in Water Resources*,  
698 28(2), 135–147. <http://doi.org/10.1016/j.advwatres.2004.09.002>
- 699 Niu, J., & Sivakumar, B. (2013). Study of runoff response to land use change in the East River basin in  
700 South China. *Stochastic Environmental Research and Risk Assessment*.  
701 <http://doi.org/10.1007/s00477-013-0690-5>  
702
- 703 Nossent, J., P. Elsen, and W. Bauwens. (2011) Sobol' sensitivity analysis of a complex environmental  
704 model. *Environmental Modelling & Software* 26.12 (2011): 1515-1525.
- 705 Pathiraja, S., Marshall, L., Sharma, A., & Moradkhani, H. (2016a). Hydrologic modeling in dynamic  
706 catchments: A data assimilation approach. *Water Resources Research*, 52, 3350–3372.  
707 <http://doi.org/10.1002/2015WR017192>
- 708 Pathiraja, S., Marshall, L., Sharma, a., & Moradkhani, H. (2016b). Detecting non-stationary hydrologic  
709 model parameters in a paired catchment system using data assimilation. *Advances in Water*  
710 *Resources*, 94, 103–119. <http://doi.org/10.1016/j.advwatres.2016.04.021>
- 711 Pianosi, F., Sarrazin, F., Wagener, T. A Matlab toolbox for Global Sensitivity Analysis, *Environmental*

- 712 *Modelling & Software*, 70, 80-85, <http://dx.doi.org/10.1016/j.envsoft.2015.04.009>.
- 713 Price, K. (2011). Effects of watershed topography, soils, land use, and climate on baseflow hydrology  
714 in humid regions: A review. *Progress in physical geography* 35.4 (2011): 465-492.  
715 <http://journals.sagepub.com/doi/abs/10.1177/0309133311402714#articleCitationDownloadCon>  
716 [tainer](http://journals.sagepub.com/doi/abs/10.1177/0309133311402714#articleCitationDownloadContainer)
- 717 Reed, P. M., Hadka, D., Herman, J. D., Kasprzyk, J. R., & Kollat, J. B. (2013). Evolutionary  
718 multiobjective optimization in water resources: The past, present, and future. *Advances in water*  
719 *resources*, 51, 438-456.
- 720 Reichle, R. H., D. B. McLaughlin, and D. Entekhabi (2002), Hydrologic Data Assimilation with the  
721 Ensemble Kalman Filter, *Am. Meteorol. Soc. - Mon. Weather Rev.*, 130(1), 103–114,  
722 [http://doi.org/10.1175/1520-0493\(2002\)130<0103:HDAWTE>2.0.CO;2](http://doi.org/10.1175/1520-0493(2002)130<0103:HDAWTE>2.0.CO;2).
- 723 Rose, S., & Peters, N. E. (2001). Effects of urbanization on streamflow in the Atlanta area (Georgia,  
724 USA): a comparative hydrological approach. *Hydrological Processes*, 15(8), 1441–1457.  
725 <http://doi.org/10.1002/hyp.218>
- 726 Saltelli, A., Ratto, M., Andres, T., Campolongo, F., Cariboni, J., Gatelli, D., Saisana, M., Tarantola, S.,  
727 (2008). *Global Sensitivity Analysis, the Primer*. Wiley.
- 728 Seibert, J., & McDonnell, J. J. (2010). Land-cover impacts on streamflow: a change-detection  
729 modelling approach that incorporates parameter uncertainty. *Hydrological Sciences Journal*,  
730 55(3), 316–332. <http://doi.org/10.1080/02626661003683264>
- 731  
732 Sun, A. Y., A. Morris, and S. Mohanty (2009), Comparison of deterministic ensemble Kalman filters for  
733 assimilating hydrogeological data, *Adv. Water Resour.*, 32(2), 280–292,  
734 <http://doi.org/10.1016/j.advwatres.2008.11.006>.
- 735 Taver, V., Johannet, a., Borrell-Estupina, V., & Pistre, S. (2015). Feed-forward vs recurrent neural  
736 network models for non-stationarity modelling using data assimilation and adaptivity.  
737 *Hydrological Sciences Journal*, 60(7–8), 1242–1265.  
738 <http://doi.org/10.1080/02626667.2014.967696>
- 739 Thanapakpawin, P., Richey, J., Thomas, D., Rodda, S., Campbell, B., & Logsdon, M. (2007). Effects of  
740 landuse change on the hydrologic regime of the Mae Chaem river basin, NW Thailand. *Journal*  
741 *of Hydrology*, 334(1-2), 215–230. <http://doi.org/10.1016/j.jhydrol.2006.10.012>
- 742  
743 Villarini, G., & Krajewski, W. F. (2008). Empirically-based modeling of spatial sampling uncertainties  
744 associated with rainfall measurements by rain gauges. *Advances in Water Resources*, 31(7),  
745 1015–1023. <http://doi.org/10.1016/j.advwatres.2008.04.007>
- 746  
747 Vu, V.T., 1993. Evaluation of the impact of deforestation to inflow regime of the Hoa Binh Reservoir  
748 in Vietnam, *Hydrology of Warm Humid Regions (Proceedings of the Yokohama Symposium,*  
749 *July 1993)*. IAHS Publ. no. 216
- 750  
751 Wang, J., Ishidaira, H., & Xu, Z. X. (2012). Effects of climate change and human activities on inflow  
752 into the Hoabinh Reservoir in the Red River basin. *Procedia Environmental Sciences*, 13, 1688-  
753 1698.

- 754 Warburton, M. L., Schulze, R. E., & Jewitt, G. P. W. (2012). Hydrological impacts of land use change in  
755 three diverse South African catchments. *Journal of Hydrology*, 414–415, 118–135.  
756 <http://doi.org/10.1016/j.jhydrol.2011.10.028>
- 757 Weerts, A. H., & El Serafy, G. Y. H. (2006). Particle filtering and ensemble Kalman filtering for state  
758 updating with hydrological conceptual rainfall-runoff models. *Water Resources Research*, 42(9),  
759 n/a-n/a. <http://doi.org/10.1029/2005WR004093>
- 760 Westra, S.; Thyer, M.; Leonard, M.; Kavetski, D.; Lambert, M. (2014). A strategy for diagnosing and  
761 interpreting hydrological model nonstationarity. *Water Resources Research*, 5090–5113.  
762 <http://doi.org/10.1002/2013WR014719>.Received
- 763 Wijesekara, G. N., Gupta, A., Valeo, C., Hasbani, J. G., Qiao, Y., Delaney, P., & Marceau, D. J. (2012).  
764 Assessing the impact of future land-use changes on hydrological processes in the Elbow River  
765 watershed in southern Alberta, Canada. *Journal of Hydrology*, 412–413, 220–232.  
766 <http://doi.org/10.1016/j.jhydrol.2011.04.018>
- 767 WWF. (2013). Ecosystems in the Greater Mekong: Past trends, current status, possible futures.
- 768 Xie, X., Meng, S., Liang, S., & Yao, Y. (2014). Improving streamflow predictions at ungauged locations  
769 with real-time updating: application of an EnKF-based state-parameter estimation strategy.  
770 *Hydrology and Earth System Sciences*, 18(10), 3923–3936. [http://doi.org/10.5194/hess-18-](http://doi.org/10.5194/hess-18-3923-2014)  
771 [3923-2014](http://doi.org/10.5194/hess-18-3923-2014)
- 772 Xu, T., and J. . Gomez-Hernandez (2016), Joint identification of contaminant source location, initial  
773 release time, and initial solute concentration in an aquifer via ensemble kalman filtering, *Water*  
774 *Resour. Res.*, 600–612, <http://doi.org/10.1002/2015WR018249>.
- 775 Yang, L., Wei, W., Chen, L., & Mo, B. (2012). Response of deep soil moisture to land use and  
776 afforestation in the semi-arid Loess Plateau, China. *Journal of Hydrology*, 475, 111–122.  
777 <http://doi.org/10.1016/j.jhydrol.2012.09.041>
- 778 Zimmermann, B., H. Elsenbeer, and J. M. De Moraes. (2006) The influence of land-use changes on soil  
779 hydraulic properties: implications for runoff generation. *Forest ecology and management* 222.1-  
780 3 (2006): 29-38.

	Pre 1994	Post 1994
<b>Land Use</b>		
<b>Evergreen Forest (including evergreen needle and evergreen leaf) (%)</b>	77%	48%
<b>Cropland (%)</b>	23%	52%
<b>Hydro-Meteorological Properties</b>		
<b>Mean Annual Rainfall (mm)</b>	1630	1660
<b>Mean Annual Runoff (mm)</b>	838	1190
<b>Mean Annual Runoff Coefficient</b>	0.5	0.7
<b>Mean Annual PET (mm)</b>	1300	1300
<b>Estimated Mean Annual BFI</b>	0.33	0.39

Table 1 Study catchment properties

782

783

784

785

786

787

788

	HYMOD	HBV
NSE [ ]	<b>0.77</b>	0.75
<i>Peak flows (<math>q &gt; 5\text{mm/d}</math>)</i>		
MAE [mm/d]	3.11	<b>2.85</b>
RMSE [mm/d]	<b>4.55</b>	4.72
<i>Medium flows (<math>1\text{ mm/d} \leq q \leq 5\text{mm/d}</math>)</i>		
MAE [mm/d]	<b>0.66</b>	0.80
RMSE [mm/d]	<b>0.86</b>	1.09
<i>Low flows (<math>q &lt; 1\text{mm/d}</math>)</i>		
MAE [mm/d]	0.35	<b>0.20</b>
RMSE [mm/d]	0.42	<b>0.34</b>

790 **Table 2 Model performance in pre-change conditions used for calibration (1975 – 1979). Bold face**  
791 **numbers correspond to the model with superior performance for the particular metric. NSE = Nash**  
792 **Sutcliffe Efficiency; MAE = Mean Absolute Error; RMSE = Root Mean Squared Error.**

793

794

795

796

	Sensitivity Index
<i>h1</i>	0.10
<i>lp</i>	0.12
<i>Maxbas</i>	0.14
<i>fcap</i>	0.18
<i>k0</i>	0.23
<i>k2</i>	0.23
<i>k1</i>	0.38
<i>beta</i>	0.41
<i>perc</i>	0.47

797 **Table 3 Variance Based Sensitivity Analysis Results for HBV parameters: first order sensitivity index**  
798 **representing the contribution of varying a single parameter to the variance of the model output.**  
799 **Lower values indicate lower sensitivity.**

800

801

802

803

804

<b>Parameters</b>						
	<b>Description</b>	<b>Units</b>	<b>Initial Sampling Distribution</b>	<b>Feasible Range</b>	$s^2$	<b>Max allowable daily rate of change (<math>m_{max}</math>)</b>
$\beta$	Soil Moisture exponent	[ ]	$N(2, 0.1)$	0 – 7	0.003	$1.8 \times 10^{-3}$
$f_{cap}$	Maximum soil moisture store depth	[mm]	$N(467, 10)$	10 – 2000	0.003	0.4
$hl1$	Threshold for generation of near surface flow	[mm]	$N(120, 10)$	0 – 400	0.003	0.1
$K0$	Near Surface Flow Routing Coefficient	[ ]	$N(0.3, 0.005)$	0.0625 – 1	0.003	$2 \times 10^{-4}$
$K1$	Interflow Routing Coefficient	[ ]	$N(0.09, 5 \times 10^{-4})$	0.02 – 0.1	0.003	$9 \times 10^{-6}$
$perc$	Percolation rate	[mm/d]	$N(1.3, 10^{-4})$	0 – 3	0.003	$10^{-3}$
$K2$	Baseflow Routing Coefficient	[ ]	$N(0.01, 10^{-6})$	$5 \times 10^{-5}$ – 0.02	0.003	$9 \times 10^{-6}$
<b>States</b>						
$sowat$	Soil Moisture Store	[mm]	$N(0,1)$	$(0, f_{cap})$		
$stw1$	Shallow Layer Store	[mm]	$N(0,1)$	$(0, \infty)$		
$stw2$	Deep Layer Store	[mm]	$N(0,0.1)$	$(0, \infty)$		

805

**Table 4 Locally Linear EnKF inputs for the HBV model case**

806

807

<b>Parameters</b>						
	<b>Description</b>	<b>Units</b>	<b>Initial Sampling Distribution</b>	<b>Feasible Range</b>	$s^2$	<b>Max allowable daily rate of change (<math>m_{max}</math>)</b>
$b$	Pareto-distributed soil storage shape parameter	[ ]	$N(0.37, 10^{-4})$	0 – 0.3	0.004	$3 \times 10^{-4}$
$c_{max}$	Maximum point soil storage depth	[mm]	$N(651, 10)$	300 – 1500	0.004	0.3
$k_q$	Quick flow Routing Coefficient	[ ]	$N(0.6, 5 \times 10^{-4})$	0.55 – 0.99	0.018	$3 \times 10^{-4}$
$k_s$	Slow flow Routing Coefficient	[ ]	$N(0.04, 5 \times 10^{-4})$	0.001 – 0.54	0.018	$4 \times 10^{-5}$
$\alpha$	Excess Runoff Splitting Parameter	[ ]	$N(0.47, 5 \times 10^{-4})$	0.001 – 0.99	0.018	$4 \times 10^{-4}$
<b>States</b>						
$S$	Soil Store	[mm]	$N(180, 0.1 \cdot 180)$	$(0, S_{max} = \frac{b c_{min} + c_{max}}{b+1})$		
$S_{q1,2,3}$	Quick Flow Stores	[mm]	$N(0,1)$	$(0, \infty)$		
$S_s$	Slow Flow Store	[mm]	$N(0,1)$	$(0, \infty)$		

808 **Table 5 Locally Linear EnKF inputs for the HYMOD model case**

809

810

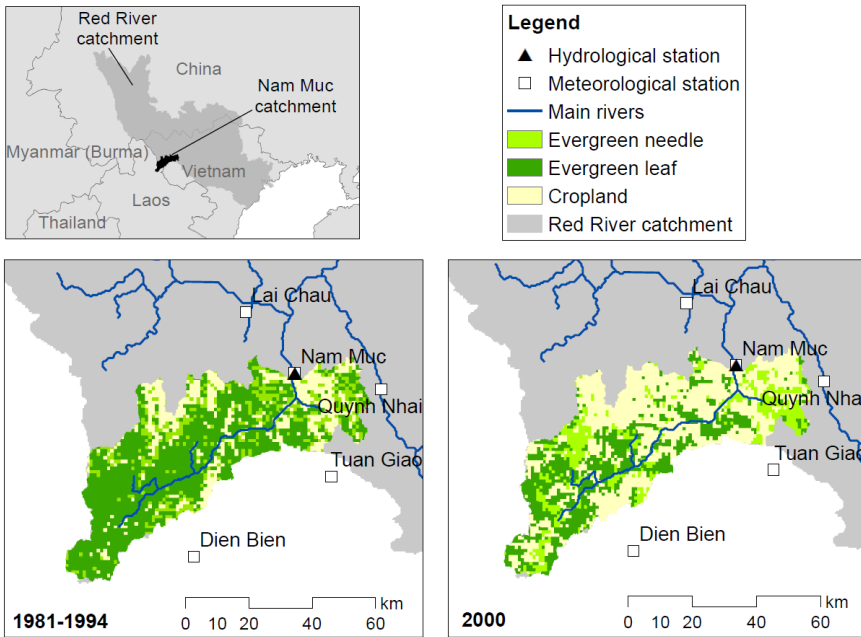
811

812

813

814 **Figures**

815

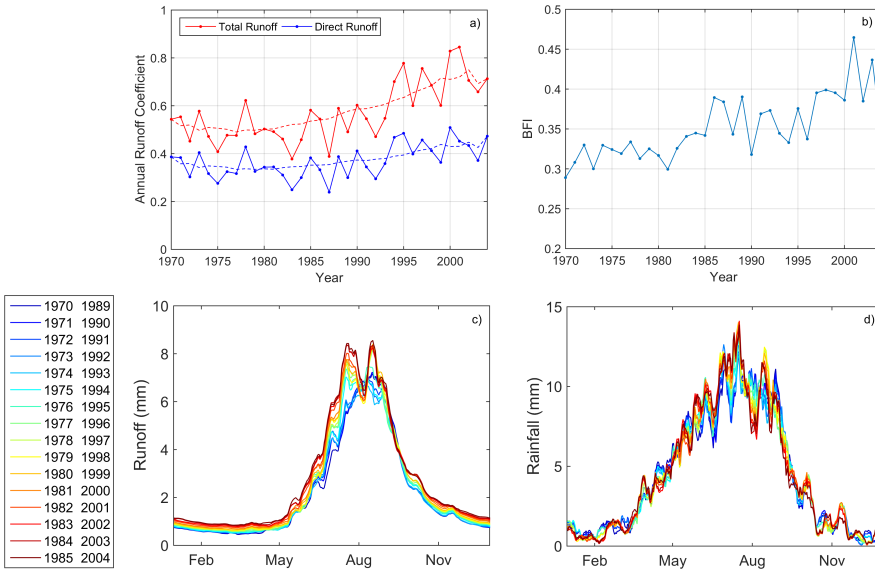


816  
817

818 **Figure 1 Study Catchment showing gauges and changes in land cover over time.**

819  
820  
821  
822  
823  
824  
825  
826  
827

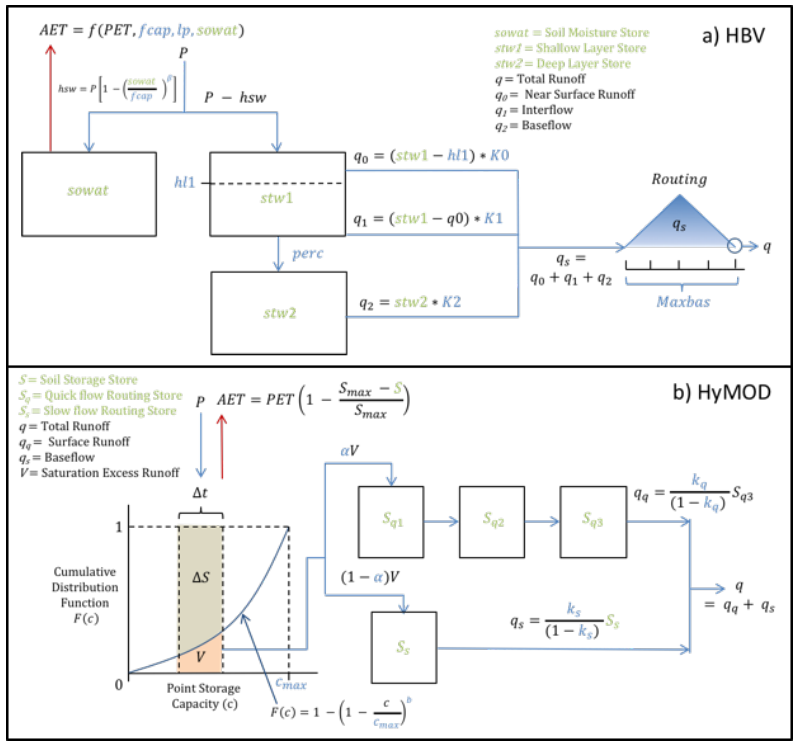
828  
829  
830



831  
832  
833

834 **Figure 2 Impact of land use change on observed streamflow: a) Annual Runoff Coefficient, b)**  
835 **Annual Baseflow Index (BFI), c) Moving Average Shifting Horizon (MASH) results for total observed**  
836 **runoff, d) MASH for observed rainfall.**

837  
838  
839  
840  
841  
842  
843  
844  
845



846

847 **Figure 3 Schematic of the models used in this study: a) HBV and b) HyMOD. Parameters are shown**  
 848 **in blue and states are shown in green.**

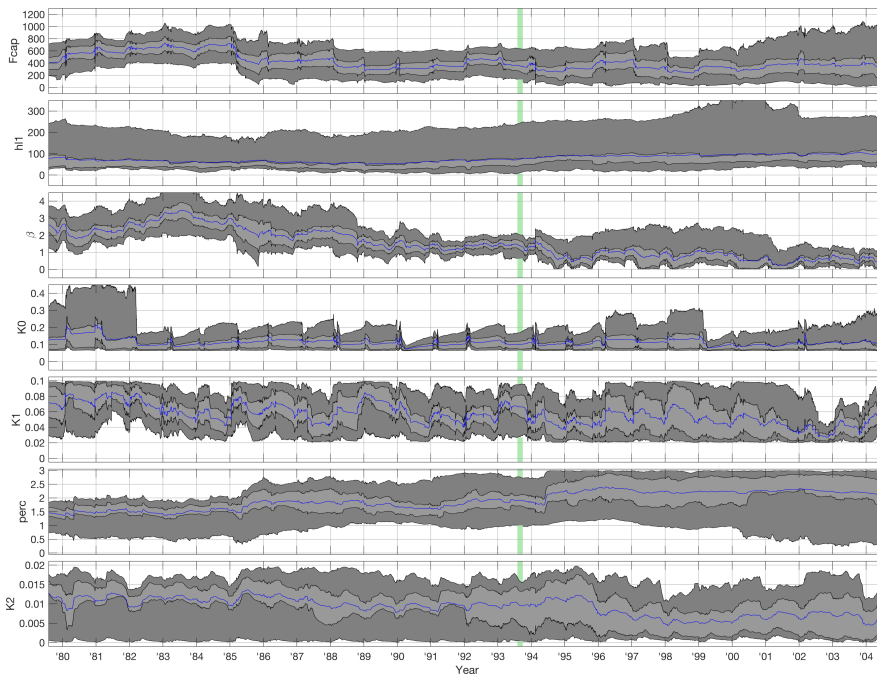
849

850

851

852

853



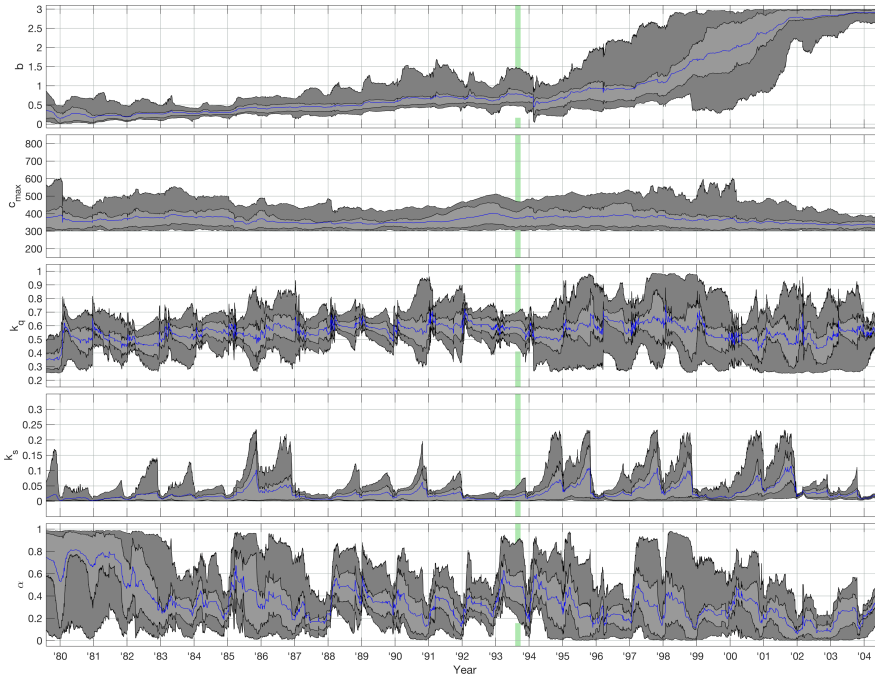
854  
 855 **Figure 4 Parameter Trajectories using the HBV model. The dark grey shaded areas indicate the**  
 856 **middle 90% of the ensemble, bounded by the 5th and 95th percentiles. The light grey shaded**  
 857 **areas indicate the middle 50% of the ensemble, bounded by the 25th and 75th percentiles. The**  
 858 **ensemble mean is indicated by the blue line. The vertical green panel indicates the assumed time**  
 859 **period of rapid deforestation.**

860

861

862

863



864

865 **Figure 5 Parameter Trajectories using the HyMOD model. The dark grey shaded areas indicate the**  
866 **middle 90% of the ensemble, bounded by the 5th and 95th percentiles. The light grey shaded**  
867 **areas indicate the middle 50% of the ensemble, bounded by the 25th and 75th percentiles. The**  
868 **ensemble mean is indicated by the blue line. The vertical green panel indicates the assumed time**  
869 **period of rapid deforestation.**

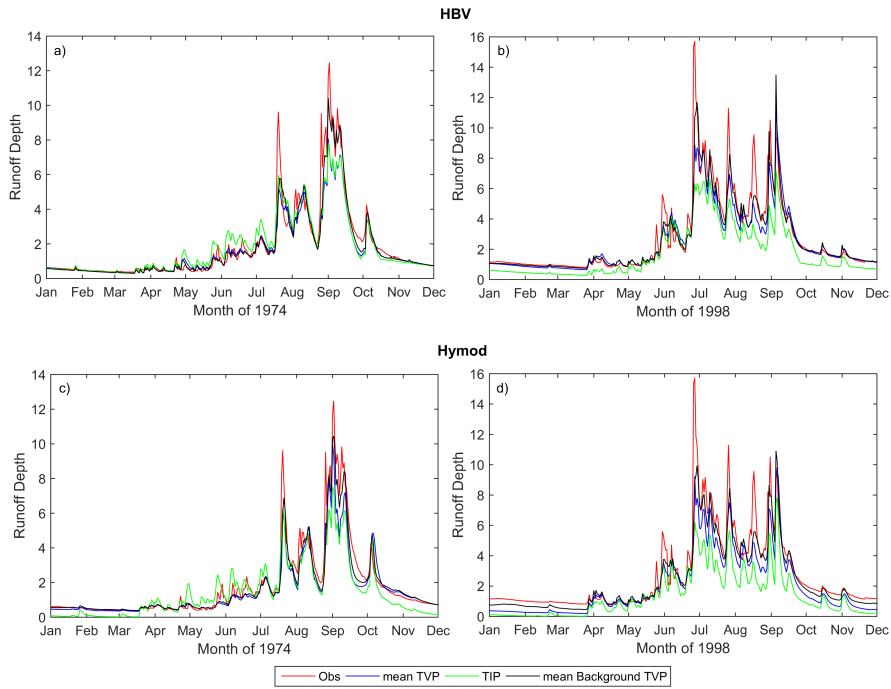
870

871

872

873

874



875

876 **Figure 6 Representative Hydrographs of background streamflow from the LL Dual EnKF (black line),**  
 877 **Time varying parameter model with no state updating (blue line), time invariant parameter model**  
 878 **with no DA (green line) and observed streamflow (red line). Results for HBV are shown in the top**  
 879 **row and HyMOD in the bottom row. A pre-change year (1974) is shown on the left and a post**  
 880 **change year (1998) on the right.**

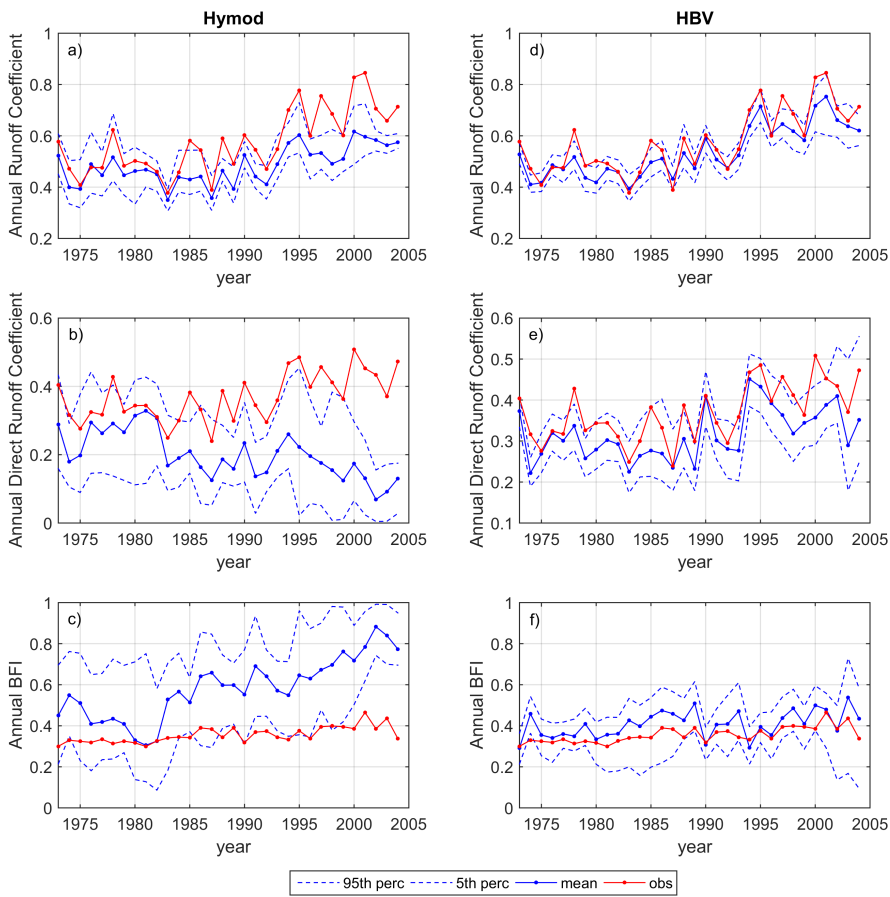
881

882

883

884

885



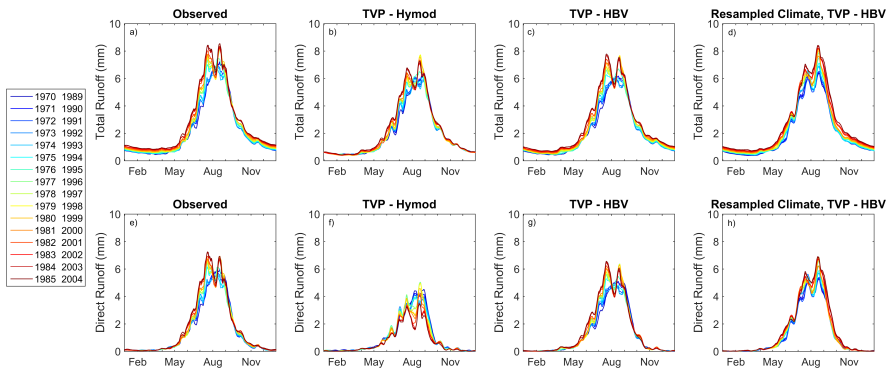
886

887 **Figure 7 Influence of time varying parameters on model output (i.e. without state updating)**  
888 **summarized in terms of the Annual Runoff Coefficient (top row), Annual Direct Runoff Coefficient**  
889 **(second row) and Annual Baseflow Index (BFI) (third row). Results for HyMOD are shown in the**  
890 **first column, HBV are shown in the second column.**

891

892

893



894

895 **Figure 8 Moving Average Shifting Horizon (MASH) results for observed streamflow (first column),**  
896 **simulated streamflow from time varying parameter model (without state DA) for HYMOD (2nd**  
897 **column), HBV (third column), resampled climate HBV (fourth column). These are split into total**  
898 **runoff (first row) and direct runoff or surface runoff (2nd row).**

899